U. S. DEPARTMENT OF THE INTERIOR
U. S. GEOLOGICAL SURVEY

Two-Dimensional Numerical Simulation of Elastic Wave Propagation for Environmental and Geotechnical Studies

Karl J. Ellefsen[1]

Open-File Report 93-714

[1] U. S. Geological Survey, MS 964, Box 25046, Denver, CO 80225

1993

ABSTRACT

To help collect, process, and interpret seismic data used in environmental and geotechnical studies, I have developed two computer programs to simulate elastic wave propagation in heterogeneous, isotropic, perfectly elastic media. Both programs are based upon the finite difference solution of the equation of motion and upon a two-dimensional mathematical model of the near-surface. One program simulates *P*- and S_V-wave propagation and the other S_H-wave propagation. Both accurately simulate propagation in the types of materials that typically exist in environmental and geotechnical studies: in a homogeneous half space, the particle velocities calculated with these finite difference methods are virtually identical to velocities calculated with exact, analytical methods. Along with the usual seismograms, each program can calculate images of the wave field as it propagates; these images show the particle velocities, the dilatational (compressional) components of the wave field and the rotational (shear) components of the wave field.

1. INTRODUCTION

An important environmental problem is determining the location and hydraulic conductivity of fractures because fractures can rapidly transport contaminants to pristine aquifers used for drinking water (Freeze and Cherry, 1979, p. 408-409). The seismic method, which uses elastic waves to probe the ground, may be the best method of detecting these fractures since it can resolve small details and the waves are strongly affected by the fractures. Other environmental problems, for which the seismic method is well suited and for the same reasons, include mapping clay layers that can trap dense non-aqueous phase liquids (Hulling and Weaver, 1991) and mapping variations in hydraulic conductivity that disperse contaminants (Hess et al., 1992). Important geotechnical problems for which the seismic method is suitable are detecting cavities in rock and fissures in soils (Hasbrouck, 1991).

What is common to these applications is that the heterogeneities — the fractures, the clay layers, the changes in lithology, and the voids — are approximately the size of or much smaller than the wave lengths of the elastic waves. The implication is that traditional seismic methods will not work well. A good example of this point is a study conducted by Taylor (1982), who found that the traditional seismic refraction method could not be used to determine the orientation of joints. Since that study some advances have been made (see e.g., Imse and Levine, 1985), but the fundamental problem of heterogeneity has not been fully addressed.

To solve the environmental and geotechnical problems, new acquisition, processing, and interpretation techniques that properly account for the heterogeneity must be developed. The key to this development is knowing how the heterogeneity affects the waves, and for this reason I have developed two computer programs to simulate elastic waves in the types of heterogeneous media that are commonly encountered in environmental and geotechnical studies.

In this report both programs are described. In the next section, I discuss the equations on which the programs are based and the implementation of those equations using the finite difference method. Then I discuss proper selection of grid spacing, temporal step size, grid size, sources, and recorded wave field. Finally, I demonstrate the accuracy of the seismograms computed with the finite difference method by comparing them to seismograms computed with exact, analytical solutions.

2. METHOD

The selection of the appropriate method for simulating elastic wave propagation depends upon two criteria. First is the size of the heterogeneity, a, compared to a wave length, λ, and is expressed as the ratio, $2\pi a/\lambda$. For typical environmental and geotechnical studies, this ratio generally ranges from 1 to 10, although it could be larger or smaller by a factor of 10. The second criterion is the propagation distance, L, compared to a wave length and is expressed as the ratio, $2\pi L/\lambda$. For typical studies, this ratio generally ranges from 10 to 100, although, again, it could be much larger or smaller. For the ranges of these two ratios, Aki and Richards (1980, p. 748-751) indicate that either finite difference methods or finite element methods may be used to simulate wave propagation. I chose the former for two reasons. First, the computer code for finite difference methods is simpler than the code for finite elements. Second, for materials with high Poisson's ratios, which are common in environmental and geotechnical studies, an accurate finite difference method has been developed whereas an accurate finite element method has not.

Three assumptions are inherent in the computer programs that I developed to simulate wave propagation. (1) The materials through which the waves propagate are isotropic. This assumption is satisfactory for soils, but probably not for rock. However, since anisotropy probably has less effect on the waves than heterogeneity in environmental and geotechnical studies, I will neglect it now. (2) The materials through which the waves propagate are perfectly elastic. This assumption is generally poor for the types of environmental studies we hope to address — soils and fractured rock have significant attenuation. In the future, I will modify the programs to account for the anelasticity of the media. (3) The mathematical models for the ground and for the source are two dimensional. To understand this assumption, imagine that a right-handed coordinate system is used to describe locations in the ground: positive x and positive y are in the horizontal plane, and positive z is downward. The properties of the ground may vary in the x and z directions, but not in the y direction. The source is along a line in the y direction, and its properties do not vary in this direction. Although the ground and the source are never two dimensional, this approximation is sometimes satisfactory.

Only the equation of motion and the stress-strain relation (Aki and Richards, 1981, p. 17 and 20) are needed to develop the equations for the computer programs. Due to invariance in the y direction, all derivatives of displacement and stress with respect to y are zero. As a result, the equation of motion and the stress-strain relation separate into two independent systems of equations:

$$\rho\partial_{tt}^2 u_x = \partial_x \tau_{xx} + \partial_z \tau_{xz} + f_x \tag{1a}$$

$$\rho\partial_{tt}^2 u_z = \partial_z \tau_{zz} + \partial_x \tau_{xz} + f_z \tag{1b}$$

$$\tau_{xx} = (\lambda + 2\mu)\partial_x u_x + \lambda\partial_z u_z + \hat{\tau}_{xx} \tag{1c}$$

$$\tau_{zz} = \lambda\partial_x u_x + (\lambda + 2\mu)\partial_z u_z + \hat{\tau}_{zz} \tag{1d}$$

$$\tau_{xz} = \mu(\partial_x u_z + \partial_z u_x) + \hat{\tau}_{xz} \tag{1e}$$

and

$$\rho\partial_{tt}^2 u_y = \partial_z \tau_{yz} + \partial_x \tau_{xy} + f_y \tag{2a}$$

$$\tau_{yz} = \mu\partial_z u_y + \hat{\tau}_{yz} \tag{2b}$$

$$\tau_{xy} = \mu\partial_x u_y + \hat{\tau}_{xy} \tag{2c}$$

where λ and μ are the Lame parameters, and ρ the density. The i, j component of the stress tensor is τ_{ij}, the i component of displacement is u_i, and the i component of the body force per unit volume is f_i. A discontinuity in a component of the stress tensor, $\hat{\tau}_{ij}$, which is used to repesent some sources. The first system describes P- and S_V-wave propagation, the second S_H-wave propagation.

I will implement a solution developed by Vireaux (1984 and 1986) using particle velocity, v_i, instead of particle displacement. The advantage of this approach is that now both systems of equations only involve first derivatives:

$$\rho\partial_t v_x = \partial_x \tau_{xx} + \partial_z \tau_{xz} + f_x \tag{3a}$$

$$\rho\partial_t v_z = \partial_z \tau_{zz} + \partial_x \tau_{xz} + f_z \tag{3b}$$

$$\partial_t \tau_{xx} = (\lambda + 2\mu)\partial_x v_x + \lambda\partial_z v_z + \partial_t \hat{\tau}_{xx} \tag{3c}$$

$$\partial_t \tau_{zz} = \lambda\partial_x v_x + (\lambda + 2\mu)\partial_z v_z + \partial_t \hat{\tau}_{zz} \tag{3d}$$

$$\partial_t \tau_{xz} = \mu\left(\partial_x v_z + \partial_z v_x\right) + \partial_t \hat{\tau}_{xz} \tag{3e}$$

and

$$\rho \partial_t v_y = \partial_z \tau_{yz} + \partial_x \tau_{xy} + f_y \tag{4a}$$

$$\partial_t \tau_{yz} = \mu \partial_z v_y + + \partial_t \hat{\tau}_{yz} \tag{4b}$$

$$\partial_t \tau_{xy} = \mu \partial_x v_y + + \partial_t \hat{\tau}_{xy} \ . \tag{4c}$$

These equations can be solved using the finite difference method. Let *i* be the index for the *x* direction, *j* for the *z* direction, and *k* for time. The stress components and particle displacements are calculated for the staggered grids shown in Figures 1 and 2, which are for the first and second systems, respectively. The derivatives are expressed with centered finite differences, and each equation is solved for the particle velocities and stress components:

$$v_x\Big|_{i,j}^{k+\frac{1}{2}} = v_x\Big|_{i,j}^{k-\frac{1}{2}} + \rho^{-1}\Big|_{i,j} \frac{\Delta t}{\Delta x}\left(\tau_{xx}\Big|_{i+\frac{1}{2},j}^{k} - \tau_{xx}\Big|_{i-\frac{1}{2},j}^{k}\right) + \rho^{-1}\Big|_{i,j} \frac{\Delta t}{\Delta z}\left(\tau_{xz}\Big|_{i,j+\frac{1}{2}}^{k} - \tau_{xz}\Big|_{i,j-\frac{1}{2}}^{k}\right) + \rho^{-1}\Big|_{i,j} \Delta t f_x\Big|_{i,j}^{k+\frac{1}{2}} \tag{5a}$$

$$v_z\Big|_{i+\frac{1}{2},j+\frac{1}{2}}^{k+\frac{1}{2}} = v_z\Big|_{i+\frac{1}{2},j+\frac{1}{2}}^{k-\frac{1}{2}} + \rho^{-1}\Big|_{i+\frac{1}{2},j+\frac{1}{2}} \frac{\Delta t}{\Delta z}\left(\tau_{zz}\Big|_{i+\frac{1}{2},j+1}^{k} - \tau_{zz}\Big|_{i+\frac{1}{2},j}^{k}\right) + \rho^{-1}\Big|_{i+\frac{1}{2},j+\frac{1}{2}} \frac{\Delta t}{\Delta x}\left(\tau_{xz}\Big|_{i+1,j+\frac{1}{2}}^{k} - \tau_{xz}\Big|_{i,j+\frac{1}{2}}^{k}\right) + \rho^{-1}\Big|_{i+\frac{1}{2},j+\frac{1}{2}} \Delta t f_z\Big|_{i+\frac{1}{2},j+\frac{1}{2}}^{k+\frac{1}{2}} \tag{5b}$$

$$\tau_{xx}\Big|_{i+\frac{1}{2},j}^{k+1} = \tau_{xx}\Big|_{i+\frac{1}{2},j}^{k} + \left(\lambda + 2\mu\right)\Big|_{i+\frac{1}{2},j} \frac{\Delta t}{\Delta x}\left(v_x\Big|_{i+1,j}^{k+\frac{1}{2}} - v_x\Big|_{i,j}^{k+\frac{1}{2}}\right) + \lambda\Big|_{i+\frac{1}{2},j} \frac{\Delta t}{\Delta z}\left(v_z\Big|_{i+\frac{1}{2},j+\frac{1}{2}}^{k+\frac{1}{2}} - v_z\Big|_{i+\frac{1}{2},j-\frac{1}{2}}^{k+\frac{1}{2}}\right) + \hat{\tau}_{xx}\Big|_{i+\frac{1}{2},j}^{k+1} - \hat{\tau}_{xx}\Big|_{i+\frac{1}{2},j}^{k} \tag{5c}$$

$$\tau_{zz}\Big|_{i+\frac{1}{2},j}^{k+1} = \tau_{zz}\Big|_{i+\frac{1}{2},j}^{k} + \lambda\Big|_{i+\frac{1}{2},j} \frac{\Delta t}{\Delta x}\left(v_x\Big|_{i+1,j}^{k+\frac{1}{2}} - v_x\Big|_{i,j}^{k+\frac{1}{2}}\right) + (\lambda+2\mu)\Big|_{i+\frac{1}{2},j} \frac{\Delta t}{\Delta z}\left(v_z\Big|_{i+\frac{1}{2},j+\frac{1}{2}}^{k+\frac{1}{2}} - v_z\Big|_{i+\frac{1}{2},j-\frac{1}{2}}^{k+\frac{1}{2}}\right) + \hat{\tau}_{zz}\Big|_{i+\frac{1}{2},j}^{k+1} - \hat{\tau}_{zz}\Big|_{i+\frac{1}{2},j}^{k} \tag{5d}$$

$$\tau_{xz}\Big|_{i,j+\frac{1}{2}}^{k+1} = \tau_{xz}\Big|_{i,j+\frac{1}{2}}^{k} + \mu\Big|_{i,j+\frac{1}{2}} \frac{\Delta t}{\Delta x}\left(v_z\Big|_{i+\frac{1}{2},j+\frac{1}{2}}^{k+\frac{1}{2}} - v_z\Big|_{i-\frac{1}{2},j+\frac{1}{2}}^{k+\frac{1}{2}}\right) + \mu\Big|_{i,j+\frac{1}{2}} \frac{\Delta t}{\Delta z}\left(v_x\Big|_{i,j+1}^{k+\frac{1}{2}} - v_x\Big|_{i,j}^{k+\frac{1}{2}}\right) + \hat{\tau}_{xz}\Big|_{i,j+\frac{1}{2}}^{k+1} - \hat{\tau}_{xz}\Big|_{i,j+\frac{1}{2}}^{k} \tag{5e}$$

and

$$v_y\Big|_{i,j}^{k+\frac{1}{2}} = v_y\Big|_{i,j}^{k-\frac{1}{2}} + \rho^{-1}\Big|_{i,j} \frac{\Delta t}{\Delta x}\left(\tau_{xy}\Big|_{i+\frac{1}{2},j}^{k} - \tau_{xy}\Big|_{i-\frac{1}{2},j}^{k}\right) + \rho^{-1}\Big|_{i,j} \frac{\Delta t}{\Delta z}\left(\tau_{yz}\Big|_{i,j+\frac{1}{2}}^{k} - \tau_{yz}\Big|_{i,j-\frac{1}{2}}^{k}\right) + \rho^{-1}\Big|_{i,j} \Delta t f_y\Big|_{i,j}^{k+\frac{1}{2}} \tag{6a}$$

$$\tau_{yz}\Big|_{i,j+\frac{1}{2}}^{k+1} = \tau_{yz}\Big|_{i,j+\frac{1}{2}}^{k} + \mu\Big|_{i,j+\frac{1}{2}} \frac{\Delta t}{\Delta z}\left(v_y\Big|_{i,j+1}^{k+\frac{1}{2}} - v_y\Big|_{i,j}^{k+\frac{1}{2}}\right) + \hat{\tau}_{yz}\Big|_{i,j+\frac{1}{2}}^{k+1} - \hat{\tau}_{yz}\Big|_{i,j+\frac{1}{2}}^{k} \tag{6b}$$

$$\tau_{xy}\Big|_{i+\frac{1}{2},j}^{k+1} = \tau_{xy}\Big|_{i+\frac{1}{2},j}^{k} + \mu\Big|_{i+\frac{1}{2},j} \frac{\Delta t}{\Delta x}\left(v_y\Big|_{i+1,j}^{k+\frac{1}{2}} - v_y\Big|_{i,j}^{k+\frac{1}{2}}\right) + \hat{\tau}_{xy}\Big|_{i+\frac{1}{2},j}^{k+1} - \hat{\tau}_{xy}\Big|_{i+\frac{1}{2},j}^{k}. \tag{6c}$$

In the grid for simulating P- and S_V-wave propagation (Figure 1), the top is a free surface that represents the surface of the ground (Aki and Richards, 1980, p. 135). The right, left, and bottom sides are transmitting boundaries that simulate wave propagation into an infinite space. The equations for the particle velocities and stress components on these four sides are derived in Appendix A. Initially all particle velocities and stress components are set to zero. At time step 1/2, the particle velocities at the interior grid points are calculated with equations 5a and 5b (which include sources represented by body forces), at the boundary points with A-4 and A-6, and at the free surface with A-7. At time step 1, the stress components at the interior grid points are calculated with equations 5c, 5d, and 5e (which include sources represented by discontinuities in components of the stress

tensor), at the boundary points with A-3 and A-5, and at the free surface with A-8. This two-step cycle is repeated until all waves of interest are recorded.

The procedure for simulating S_h-wave propagation is similar. The top of the grid (Figure 2) models a free surface; the left, right, and bottom sides transmitting boundaries. The equations for the free surface and these boundaries are in Appendix B. At half time steps, the y component of particle velocity at the interior grid points is calculated with equation 6a (which include sources represented by body forces) and at the free surface with B-3. At all integral time steps, the stress components at the interior points are calculated with equations 6b and 6c (which include sources represented by discontinuities in components of the stress tensor) and at the boundary points with B-1 and B-2.

3. DISCUSSION OF THE METHOD

3.1 Grid Spacing

Ideally, the waves that are simulated during a finite difference solution of the wave equation propagate at the same speed as that determined by the elastic moduli and density. However, the grid causes velocity dispersion, and consequently the spacing between the nodes on the grid must be properly selected to minimize this dispersion. Previous researchers (see e.g., Aki and Richards, 1980, p. 773-788) have found that from analyzing the dispersion of body waves in a homogeneous medium they have enough information to properly select the grid spacing for an accurate simulation of all waves.

In Appendix C I derive analytical expressions for the dispersion of the phase and group velocities of simulated P- and S_v-waves. These velocities are normalized by the exact velocities to make the results easier to compare. In addition to depending upon the exact velocities, the normalized velocities for the simulated waves depend upon the grid spacing per wave length, the direction of propagation with respect to the grid, and γ, a parameter related to the temporal step size (see section 3.2). For all calculations, I set γ to 0.95, a typical value. I made the grid spacing in the x and z directions the same, a common practice. Consequently, the normalized velocities are symmetric with respect to these axes — knowing the velocity when the direction of propagation is between 0° and 45° is enough information to predict it for any direction.

The dispersion of phase velocity of the P-wave (Figure 3) is negligibly small at all angles when the normalized grid spacing is less than 0.2. In contrast, the dispersion of its group velocity (Figure 4) is only small when the spacing is less than 0.1; it is severe above approximately 0.3 for small angles. I calculated the dispersion for the S_v-wave at extreme values of Poisson's ratio: 0.25, which is lower than that of steel, and 0.499, which is higher than that of a poorly consolidated soil. For both cases, the dispersion of its phase velocity (Figures 5 and 6) is small when the spacing is less than 0.2. The dispersion of its group velocity is small when the spacing is less than 0.1 but is large at all angles when the spacing is greater than 0.3. A rule-of-thumb that can made from these examples is that the

normalized grid spacing must be less than 0.1 for accurate simulation of body waves. In practice, I apply this rule to surface waves too; I obtain accurate results as I will demonstrate with an example in section 4. The formulas for the dispersion of the phase and group velocities of an S_h-wave (Appendix D) are identical to those for a P-wave. Consequently, the rule-of-thumb for the P- and S_v-waves applies to S_h-waves as well.

These calculations demonstrate that in a material with a high Poisson's ratio, which commonly occurs in soils, wave propagation can be accurately simulated with a staggered finite difference grid. Standard grids give inaccurate results for this situation (Marfurt, 1984), and for this reason I chose the staggered grid.

3.2 Temporal Step Size

The temporal step size, Δt, must be small enough to make the finite difference solution stable — if it too large then the solution is unstable, which is manifested by inaccurate values for particle velocities and stress components. In Appendix C, I derive a stability condition for the simulation of P- and S_v-wave propagation:

$$\Delta t = \frac{\gamma \Delta x}{\alpha \sqrt{2}}, \tag{7}$$

where α is the highest speed of P-wave propagation in the model and γ is a number less than 1. (For this formula, I assume that the spacing in the z direction equals that in the x direction.) To minimize the number of calculations, I make γ close to 1, say 0.95. In Appendix D, I derive a stability condition for the simulation of S_h-wave propagation; it is identical to the previous equation except the α is replaced by β, the highest speed of S_h-wave propagation in the model

3.3 Size of Grid

When selecting the size of the grid, several requirements must be considered. The grid must be large enough to simulate completely all waves of interest that are created by heterogeneities. If a highly accurate simulation is needed, then the grid must be large enough that the reflections from the right, left, and bottom boundaries do not interfere with the original waves. On the other hand, the grid must not be so large that the capacity of the computer memory is being exceeded. Finally, the grid must be as small as possible to minimize the amount of computation.

3.4 Sources

With a suitable choice of body forces or discontinuities in components of the stress tensor, any field source can be accurately simulated. A blow to a metal plate with a downward swing of a hammer and a vibroseis source should be represented by a vertical body force at single grid point on the free surface. A bullet entering the ground should be represented by a vertical body force at single grid point slightly below the free surface. A blow to a metal plate with a sidewards swing of a hammer — the so-called golf shoe developed by

Hasbrouck (1992, oral commun.) — should be represented by a horizontal body force at single grid point on the free surface. An explosion, which might be caused by dynamite, should be represented by discontinuities in two components of the stress tensor, $\hat{\tau}_{xx}$ and $\hat{\tau}_{zz}$, slightly below the free surface.

Because representing a source as a discontinuity in one or more components of the stress tensor is difficult to intuit, some comments are necessary. This source is an excess of a stress component in a small volume centered at the point of application; the underlying theory of such sources is outlined in Aki and Richards (1980, p. 57-60). Approximating the volume by a point is valid because its diameter is small compared to the shortest wave lengths that are typical in environmental and geotechnical studies. Sometimes considering this source in terms of equivalent body forces is helpful The mathematical definition of the these equivalents (Aki and Richards, 1980, p. 61) shows that they equal the moment tensor times the spatial derivative of a delta function; the later term indicates that these are force couples. Another way of thinking about these equivalents, which is imprecise but conceptually easy, is that they are tractions on opposite sides of the volume. Because the volume is symmetric, the tractions point in opposite directions making them force couples.

3.5 Recorded Wave Field

The wave field may be studied by examining the components of either the particle velocity or the stress. Heretofore I have only examined the particle velocity because it is measured by most geophones (White, 1983, p. 231) that are used today. Both quantities may be recorded as either seismograms or snapshots of the wave field. Seismograms are important because field data are recorded this way. Snapshots, which are simply images of the wave field constructed from one component of the particle velocity or stress, are important because they clearly show how heterogeneity affects the propagating waves. For P- and S_V-wave propagation, I have found that these snapshots are easier to analyze if they are processed to show the compressional and shear components, which are computed from the divergence and curl, respectively, of the particle velocities (Bullen, 1979, p. 73).

4. TESTS OF ACCURACY

I tested the accuracy of the finite difference methods by comparing their solutions to exact, analytical solutions. For the results that I will present here, the models are homogeneous half-spaces — the most complicated models for which analytical solutions exist (Appendices E and F). Because these models contain a free surface, the tests also evaluate the accuracy of the free surface boundary.

For the test of P- and S_V-wave propagation, the explosive source, which is 2 m below the surface, is represented by discontinuities in two components of the stress tensor, $\hat{\tau}_{xx}$ and $\hat{\tau}_{zz}$ (Figure 9). The source wavelet is the first derivative of a Gaussian (Kelly et al., 1976)

for which the frequencies range from approximately 1 to 50 Hz and the duration is 0.184 s. The receivers are evenly spaced along the surface. The left, right, and bottom transmitting boundaries are far enough away that any reflections from them will be not recorded by the receivers. The finite difference solutions for the x and z components of the particle velocity closely match the analytical solutions (Figure 10 a and b). The matches in other tests with infinite homogeneous models, which are much less complicated, are also excellent.

For the test of SH-wave propagation, the model and source-receiver configuration are identical with two exceptions (Figure 11). First, the sources and receivers are 5 m below the surface and are closer together. Second, the source is a body force in the y direction, f_y. Again, the finite difference solution for the particle velocity closely matches the analytical solution (Figure 12). The match in another test with an infinite homogeneous model is also excellent.

6. ACKNOWLEDGMENTS

W. Hasbrouck encouraged me to develop these programs. M. Prange and I discussed finite difference methods in detail; he also gave me some of his computer code, which helped me write my own.

7. REFERENCES

Aki, K., and Richards, P. G., 1980, Quantitative seismology: Theory and methods, vol 1 and vol. 2: San Francisco, W. H. Freeman and Co., 932 p.

Arfken, G., 1970, Mathematical Methods for Physicists: London, Academic Press, Inc., 815 p.

Bullen, K. E., 1979, An introduction to the theory of seismology: New York, Cambridge University Press, 381 p.

Freeze, R. A., and Cheery, J., A., 1979, Groundwater: Englewood Cliffs, New Jersey, Prentice Hall, Inc., 604 p.

Gilbert, F., and Knopoff, L., 1961, The directivity problem for a buried line source: Geophysics, v. 26, p. 626-634.

Hasbrouck, W. P., 1991, Four shallow-depth, shear-wave feasibility studies: Geophysics, v. 56, p. 1875-1885.

Hess, K. M., Wolf, S. H., Celia, M. A., 1992, Large scale natural gradient tracer test in sand and gravel, Cape Cod, Massachusetts, 3. Hydraulic conductivity variability and calculated macrodispersivitites: Water Resources Research, vol. 28, p. 2011-2027.

Hulling, S. G., and Weaver, J. W., 1991, Dense nonaqueous phase liquids: U. S. Environmental Protection Agency, EPA/540/4-91-002.

Imse, J. P., and Levine, E. N., 1985, Conventional and state-of-the-art geophysical techniques for fracture detection: Proceedings of the National Well Water Association Second Annual Eastern Regional Ground Water Conference, Portland, Maine, p. 261-276.

Kausel, E., 1988, Local transmitting boundaries: Journal of Engineering Mechanics, v. 114, p. 1011-1027.

Kelly, K. R., Ward, R. W., Treitel, S., and Alford, R. M., 1976, Synthentic seismograms: A finite difference approach: Geophysics, v. 41, p. 2-27.

Lathi, B. P., 1965, Signals, Systems, and Communication: New York, John Wiley and Sons, Inc., 607 p.

Lysmer, J., and Kuhlemeyer, R. L., 1969, Finite dynamic model for infinite media: Journal of the Engineering Mechanics Division, Proceedings of the American Society of Civil Engineers, v. 95, p. 859-877.

Marfurt, K. J., 1984, Accuracy of finite difference and finite element modeling of the scalar and elastic wave equations: Geophysics, v. 49, p. 533-549.

Taylor, R. W., 1982, Evaluation of geophysical surface methods for measuring hydrological variables in fractured rock units: U. S. Bureau of Mines Open File Report 17-84, 145 p.

Vireaux, J. 1984, Sh wave propagation in heterogeneous media: Velocity-stress finite difference method: Geophysics, v. 49, p. 1933-1942.

Vireaux, J. 1986, P-Sv wave propagation in heterogeneous media: Velocity-stress finite difference method: Geophysics, v. 51, p. 889-901.

White, J. E., 1983, Underground sound, Application of seismic waves: New York, Elsevier Science Publishers, B. V., 253 p.

APPENDIX A
TRANSMITTING BOUNDARIES AND FREE SURFACE, P- AND S_V-WAVES

In this appendix I derive the equations for the transmitting boundaries and the free surface that are used in the simulation of P- and S_V-wave propagation on a staggered grid. These equations are new although Lysmer and Kuhlemeyer (1969) developed similar transmitting boundaries for a standard grid. The equations for the free surface were originally developed by M. Prange (1992, oral commun.).

The transmitting boundary on the right edge of the grid (Figure 1) is simulated with special expressions for the particle velocities and stress components at the edge nodes. To determine what expressions are needed here, examine the second column of nodes from the right edge of the grid. In this column v_x and τ_{xz} are computed using equations 5a and 5c, which can be used only if τ_{xx} and v_z are known edge nodes. Therefore, expressions for τ_{xx} and v_z must be developed that simulate a boundary. The derivation for the former quantity begins with equation 3c without the source term, and a planar body wave is assumed to be incident on the boundary. Expressing the planar wave in the frequency-wavenumber domain (Aki and Richards, 1980, p. 130-133), this equation becomes:

$$\tilde{\tau}_{xx} = (\lambda + 2\mu)\left(-\frac{\bar{k}_x}{\omega}\right)\tilde{v}_x + \lambda\left(-\frac{\bar{k}_z}{\omega}\right)\tilde{v}_z \qquad \text{(A-1)}$$

where $\bar{k}_x$ and $\bar{k}_z$ are the x and z components of the wavenumber, and ω the frequency. The variables with the tildes are Fourier components. The particle velocity of a P-wave moving principally in the x direction will be in the x direction. For this reason, $\bar{k}_x/\omega$ can be replaced by $\cos\theta/\alpha$ where θ is the angle between the wave normal and the x axis and α is the speed of the wave. Similarly, the particle velocity of an S_V-wave moving principally in the x direction will be in the z direction. For this reason, $\bar{k}_z/\omega$ can be replaced by $\sin\theta/\beta$ where β is the speed of the wave. After these substitutions, equation A-1 is transformed back to the time-space domain:

$$\tau_{xx} = (\lambda + 2\mu)\left(-\frac{\cos\theta}{\alpha}\right)v_x + \lambda\left(-\frac{\sin\theta}{\beta}\right)v_z. \qquad \text{(A-2)}$$

Because the source is often near the center of the grid, θ is small. For this case, $\cos\theta \approx 1$ and $\sin\theta \approx 0$. With these approximations, the final equation for τ_{xx} is

$$\tau_{xx} \approx -\rho\alpha v_x. \qquad \text{(A-3)}$$

In this equation, I use the value of v_x in the second column from the right. The derivation for v_z begins with equation A-3 without the source term, and because it is similar to the previous derivation I will only present the result:

$$v_z \approx -\frac{1}{\rho\beta}\tau_{xz} \tag{A-4}$$

In this equation, I use the value of τ_{xz} in the second column from the right.

For the transmitting boundary on the left edge of the grid, the derivations are identical to what I just presented except that $\cos\theta \approx -1$. Therefore the equations for τ_{xx} and v_z on this side are identical to equations A-3 and A-4 except that the minus signs are omitted.

For the transmitting boundary on the bottom of the grid, expressions for τ_{xz} and v_z are needed at the bottom nodes. The derivations begin with equations 3b and 3f without the source terms, and because they are similar to what I just presented I will not repeat them. The only significant difference is in the approximation of the angle: θ is close to 90° making $\cos\theta \approx 0$ and $\sin\theta \approx 1$. The final equation for τ_{xz} is

$$\tau_{xz} \approx -\rho\beta v_x, \tag{A-5}$$

and for v_z

$$v_z \approx -\frac{1}{\rho\beta}\tau_{zz}\ . \tag{A-6}$$

The advantages of my implementation of the transmitting boundaries over other implementations (see e.g., Kausel, 1988) are that they are easy to translate into computer code, require little computer memory, and work well in heterogeneous media. The disadvantage of my implementation is that the waves hitting the boundary at large incidence angles (i.e., between approximately 60 and 90°) are partially reflected. Nonetheless, for the simulations that I have conducted this disadvantage has not caused any significant problems.

On the free surface, v_x, τ_{xx}, and τ_{zz} must be computed for the finite difference solution of the wave equation (Figure 1). By the definition of a free surface (Aki and Richards, 1980, p. 135), τ_{zz} and τ_{xz} are zero, and so τ_{zz} is simply set to zero here as the solution is computed. To calculate v_x, the finite difference approximation of equation 3a is changed. The difference in τ_{xz} is taken between the surface and one-half grid spacing below the surface ($j = \frac{1}{2}$); the finite difference equation is

$$\begin{aligned} v_x\Big|_{i,0}^{k+\frac{1}{2}} = v_x\Big|_{i,0}^{k-\frac{1}{2}} + \rho^{-1}\Big|_{i,0}\frac{\Delta t}{\Delta x}\left(\tau_{xx}\Big|_{i+\frac{1}{2},0}^{k} - \tau_{xx}\Big|_{i-\frac{1}{2},0}^{k}\right) + \\ \rho^{-1}\Big|_{i,0}\frac{2\Delta t}{\Delta z}\left(\tau_{xz}\Big|_{i,\frac{1}{2}}^{k}\right) + \rho^{-1}\Big|_{i,0}\Delta t f_x\Big|_{i,0}^{k+\frac{1}{2}} \end{aligned} \tag{A-7}$$

To calculate τ_{xx}, a modification of equation 3c is used. The problem with a straightforward implementation of this equation is that $\partial_z v_z$ is not known. To overcome

this problem equation 3d without the source term is used: after setting τ_{zz} to zero, it is solved for $\partial_z v_z$. This expression is substituted into equation 3c, and after some algebra, the result is

$$\partial_t \tau_{xx} = \frac{4\mu(\lambda+\mu)}{\lambda+2\mu}\partial_x v_x + \delta_{xx}. \qquad \text{(A-8)}$$

This equation is implemented with centered finite differences.

APPENDIX B
TRANSMITTING BOUNDARIES AND FREE SURFACE, S_h-WAVES

In this appendix I derive the equations for the transmitting boundaries and the free surface that are used in the simulation of S_h-wave propagation on a staggered grid. These equations are new. Because the derivations are similar to those for P- and S_v-waves (Appendix A), I will omit redundant details.

For the transmitting boundary on the right edge of the grid (Figure 2), a special expression for τ_{xy} is needed to simulate propagation into an infinite space. Beginning with equation 4b without the source term and following a derivation virtually identical to that in Appendix A, this expression for the stress component is derived:

$$\tau_{xy} \approx -\rho\beta v_y. \qquad \text{(B-1)}$$

For the boundary on the left edge, τ_{xy} is the same except that the minus sign is omitted. For the bottom of the grid, a special expression for τ_{zy} is needed. The derivation begins with equation 4c without the source term, and after some algebra this expression is derived:

$$\tau_{yz} \approx -\rho\beta v_y. \qquad \text{(B-2)}$$

These transmitting boundaries have the same advantages and disadvantages that the boundaries for P- and S_v-waves have (Appendix A).

On the free surface, v_y and τ_{xy} must be computed (Figure 2). Here equation 4c for τ_{xy} can be used without any changes. To calculate v_y, the difference in τ_{yz} is taken between the surface and one-half grid spacing below the surface ($j = ½$); the new finite difference equation is

$$v_y\Big|_{i,0}^{k+\frac{1}{2}} = v_y\Big|_{i,0}^{k-\frac{1}{2}} + \rho^{-1}\Big|_{i,0}\frac{\Delta t}{\Delta x}\left(\tau_{xy}\Big|_{i+\frac{1}{2},0}^{k} - \tau_{xy}\Big|_{i-\frac{1}{2},0}^{k}\right) + \rho^{-1}\Big|_{i,0}\frac{2\Delta t}{\Delta z}\left(\tau_{zy}\Big|_{i,\frac{1}{2}}^{k}\right) + \rho^{-1}\Big|_{i,0}\Delta t f_y\Big|_{i,0}^{k+\frac{1}{2}} \qquad \text{(B-3)}$$

APPENDIX C
DISPERSION AND STABILITY, P- AND S_V-WAVES

In this appendix I derive, for P- and S_V-waves, equations to compute the dispersion of their phase velocities, equations to compute the dispersion of their group velocities, and an equation that must be satisfied for a stable solution. The equations and derivations for the group velocities are new. The other equations were presented by Vireaux (1986) without any derivations; here I give the complete derivations.

First I will derive the dispersion equations for P- and S_V-waves. Assume that a planar, elastic wave is propagating through a homogeneous medium. Because any wave can be expressed an a linear combination of planar waves (see e.g., Aki and Richards, 1980, p. 194-200), detailed insight into the behavior of any wave can be obtained by examining the behavior of a planar wave. The components of the particle velocity and stress at location i, j and time k can be expressed in terms of related components at location 0,0 and time 0:

$$\begin{pmatrix} v_x \\ v_z \\ \tau_{xx} \\ \tau_{zz} \\ \tau_{xz} \end{pmatrix}^k_{i,j} = \begin{pmatrix} v_x \\ v_z \\ \tau_{xx} \\ \tau_{zz} \\ \tau_{xz} \end{pmatrix}^0_{0,0} \exp\left[\imath\left(\bar{k}_x i\Delta x + \bar{k}_z j\Delta z - \omega k\Delta t\right)\right] \tag{C-1}$$

where $\bar{k}_x$ and $\bar{k}_z$ are the x and z components of the wavenumber, and ω the frequency.

Similar expressions can be readily developed for a plane wave at $k+\frac{1}{2}$, $i+\frac{1}{2}$, etc. Such expressions are substituted into equations 5a, 5b, 5c, 5d, and 5e, and the resulting system is

$$0 = \mathbf{M}\begin{pmatrix} v_x \\ v_z \\ \tau_{xx} \\ \tau_{zz} \\ \tau_{xz} \end{pmatrix}^0_{0,0} \exp\left[\imath\left(\bar{k}_x i\Delta x + \bar{k}_z j\Delta z - \omega k\Delta t\right)\right] \tag{C-2}$$

where the elements of $\mathbf{M}$ are

$$m_{11} = \frac{1}{\Delta t}\left(e^{\imath\omega\Delta t/2} - e^{-\imath\omega\Delta t/2}\right) \tag{C-3a}$$

$$m_{12} = 0 \tag{C-3b}$$

$$m_{13} = \frac{1}{\rho \Delta x}\left(e^{\iota \bar{k}_x \Delta x/2} - e^{-\iota \bar{k}_x \Delta x/2}\right) \tag{C-3c}$$

$$m_{14} = 0 \tag{C-3d}$$

$$m_{15} = \frac{1}{\rho \Delta z}\left(e^{\iota \bar{k}_z \Delta z/2} - e^{-\iota \bar{k}_z \Delta z/2}\right) \tag{C-3e}$$

$$m_{21} = 0 \tag{C-3f}$$

$$m_{22} = \frac{1}{\Delta t}\left(e^{\iota \omega \Delta t/2} - e^{-\iota \omega \Delta t/2}\right) e^{\iota \bar{k}_x \Delta x/2} e^{\iota \bar{k}_z \Delta z/2} \tag{C-3g}$$

$$m_{23} = 0 \tag{C-3h}$$

$$m_{24} = \frac{1}{\rho \Delta z}\left(e^{\iota \bar{k}_z \Delta z/2} - e^{-\iota \bar{k}_z \Delta z/2}\right) e^{\iota \bar{k}_x \Delta x/2} e^{\iota \bar{k}_z \Delta z/2} \tag{C-3i}$$

$$m_{25} = \frac{1}{\rho \Delta t}\left(e^{\iota \bar{k}_x \Delta x/2} - e^{-\iota \bar{k}_x \Delta x/2}\right) e^{\iota \bar{k}_x \Delta x/2} e^{\iota \bar{k}_z \Delta z/2} \tag{C-3j}$$

$$m_{31} = \frac{\lambda + 2\mu}{\Delta x}\left(e^{\iota \bar{k}_x \Delta x/2} - e^{-\iota \bar{k}_x \Delta x/2}\right) e^{\iota \bar{k}_x \Delta x/2}\ e^{-\iota \omega \Delta t/2} \tag{C-3k}$$

$$m_{32} = \frac{\lambda}{\Delta z}\left(e^{\iota \bar{k}_z \Delta z/2} - e^{-\iota \bar{k}_z \Delta z/2}\right) e^{-\iota \omega \Delta t/2} e^{\iota \bar{k}_x \Delta x/2} \tag{C-3l}$$

$$m_{33} = \frac{1}{\Delta t}\left(e^{\iota \omega \Delta t/2} - e^{-\iota \omega \Delta t/2}\right) e^{-\iota \omega \Delta t/2} e^{\iota \bar{k}_x \Delta x/2} \tag{C-3m}$$

$$m_{34} = 0 \tag{C-3n}$$

$$m_{35} = 0 \tag{C-3o}$$

$$m_{41} = \frac{\lambda}{\Delta x}\left(e^{\iota \bar{k}_x \Delta x/2} - e^{-\iota \bar{k}_x \Delta x/2}\right) e^{-\iota \omega \Delta t/2} e^{\iota \bar{k}_x \Delta x/2} \tag{C-3p}$$

$$m_{42} = \frac{\lambda + 2\mu}{\Delta z}\left(e^{\iota \bar{k}_z \Delta z/2} - e^{-\iota \bar{k}_z \Delta z/2}\right) e^{-\iota \omega \Delta t/2} e^{\iota \bar{k}_x \Delta x/2} \tag{C-3q}$$

$$m_{43} = 0 \tag{C-3r}$$

$$m_{44} = \frac{1}{\Delta t}\left(e^{\iota \omega \Delta t/2} - e^{-\iota \omega \Delta t/2}\right) e^{-\iota \omega \Delta t/2} e^{\iota \bar{k}_x \Delta x/2} \tag{C-3s}$$

$$m_{45} = 0 \tag{C-3t}$$

$$m_{51} = \frac{\mu}{\Delta z}\left(e^{\imath \bar{k}_z \Delta z/2} - e^{-\imath \bar{k}_z \Delta z/2}\right) e^{-\imath \omega \Delta t/2}\ e^{\imath \bar{k}_z \Delta z/2} \tag{C-3u}$$

$$m_{52} = \frac{\mu}{\Delta x}\left(e^{\imath \bar{k}_x \Delta x/2} - e^{-\imath \bar{k}_x \Delta x/2}\right) e^{-\imath \omega \Delta t/2} e^{\imath \bar{k}_z \Delta z/2} \tag{C-3v}$$

$$m_{53} = 0 \tag{C-3w}$$

$$m_{54} = 0 \tag{C-3x}$$

$$m_{55} = \frac{1}{\Delta t}\left(e^{\imath \omega \Delta t/2} - e^{-\imath \omega \Delta t/2}\right) e^{-\imath \omega \Delta t/2} e^{\imath \bar{k}_z \Delta z/2} \tag{C-3y}$$

Equation C-2 has a non-trivial solution only if $\det \mathbf{M} = 0$. After much algebra, this equation is:

$$0 = T^4 + T^2\left[-\left(\alpha^2 + \beta^2\right)\left(X^2 + Z^2\right)\right] + \left[\alpha^2 \beta^2 \left(X^4 + X^2 Z^2 + Z^4\right)\right] \tag{C-4}$$

where

$$T = \frac{1}{\Delta t}\sin\left(\frac{\omega \Delta t}{2}\right) \tag{C-5a}$$

$$X = \frac{1}{\Delta x}\sin\left(\frac{\bar{k}_x \Delta x}{2}\right) \tag{C-5b}$$

$$Z = \frac{1}{\Delta z}\sin\left(\frac{\bar{k}_z \Delta z}{2}\right) \tag{C-5c}$$

$$\alpha = \sqrt{\frac{\lambda + 2\mu}{\rho}} \tag{C-6a}$$

$$\beta = \sqrt{\frac{\mu}{\rho}}. \tag{C-6b}$$

The last two equations are the formulas for the velocities of the P- and S_V-waves, respectively.

Equation C-4, which is quadratic in T^2, is solved for this quantity:

$$T^2 = \alpha^2\left(X^2 + Z^2\right) \tag{C-7}$$

and

$$T^2 = \beta^2\left(X^2 + Z^2\right). \tag{C-8}$$

Substituting equations C-5a, C-5b, and C-5c into these two yields the dispersion relations for the P- and S_V-waves:

$$\frac{1}{\Delta t^2}\sin^2\left(\frac{\omega\Delta t}{2}\right)=\frac{\alpha^2}{\Delta x^2}\sin^2\left(\frac{\bar{k}_x\Delta x}{2}\right)+\frac{\alpha^2}{\Delta z^2}\sin^2\left(\frac{\bar{k}_z\Delta z}{2}\right) \tag{C-9}$$

and

$$\frac{1}{\Delta t^2}\sin^2\left(\frac{\omega\Delta t}{2}\right)=\frac{\beta^2}{\Delta x^2}\sin^2\left(\frac{\bar{k}_x\Delta x}{2}\right)+\frac{\beta^2}{\Delta z^2}\sin^2\left(\frac{\bar{k}_z\Delta z}{2}\right), \tag{C-10}$$

respectively.

These dispersion equations are easier to use if some simple substitutions are made: (1) Set $\Delta x=\Delta z$. (2) Let H be the grid spacing per wave length, $\Delta x/\lambda$. (3) Express $\bar{k}_x$ as $2\pi\cos\theta/\lambda$ where θ is the angle from the x axis. (4) Similarly, express $\bar{k}_z$ as $2\pi\sin\theta/\lambda$. (5) For the P-wave, express ω as $2\pi\alpha_n/\lambda$ where α_n is the phase velocity of the calculated wave. (6) Use equation C-18 for Δt. After some algebra, the phase velocity of the calculated P-wave normalized by the true phase velocity is

$$\frac{\alpha_n}{\alpha}=\frac{\sqrt{2}}{\pi\gamma H}\arcsin\left\{\frac{\gamma}{\sqrt{2}}\left[\sin^2(\pi H\cos\theta)+\sin^2(\pi H\sin\theta)\right]^{1/2}\right\}. \tag{C-11}$$

Similar substitutions are made for the S_V-wave, and the result is

$$\frac{\beta_n}{\beta}=\frac{\alpha\sqrt{2}}{\beta\pi\gamma H}\arcsin\left\{\frac{\beta\gamma}{\alpha\sqrt{2}}\left[\sin^2(\pi H\cos\theta)+\sin^2(\pi H\sin\theta)\right]^{1/2}\right\}. \tag{C-12}$$

To derive the equations for the dispersion of the group velocity, equations C-9 and C-10 are differentiated with respect to the wavenumber, k. Again, the results are easier to use if the same six substitutions are made. Denote $\partial\omega/\partial k$ as α_n^g and α as α^g because the medium is not dispersive. After some algebra, the group velocity of the calculated P-wave normalized by the true group velocity is

$$\frac{\alpha_n^g}{\alpha^g}=\frac{(\sin\theta+\cos\theta)\sin(2\pi H\cos\theta)}{2\cos\left(\frac{\alpha_n}{\alpha}\frac{\pi\gamma H}{\sqrt{2}}\right)\left[\sin^2(\pi H\cos\theta)+\sin^2(\pi H\sin\theta)\right]^{1/2}}. \tag{C-13}$$

The group velocity of the calculated S_V-wave normalized by the true group velocity is calculated similarly, and the result is

$$\frac{\beta_n^g}{\beta^g} = \frac{(\sin\theta + \cos\theta)\sin(2\pi H\cos\theta)}{2\cos(\frac{\beta_n}{\beta}\frac{\beta\pi\gamma H}{\alpha\sqrt{2}})\left[\sin^2(\pi H\cos\theta) + \sin^2(\pi H\sin\theta)\right]^{1/2}}. \qquad \text{(C-14)}$$

I will now use the equations C-9 and C-10 to derive the condition for stability. Because the frequency must be real,

$$1 \geq \sin\left(\frac{\omega\Delta t}{2}\right). \qquad \text{(C-15)}$$

Applying this condition to the dispersion equations yields:

$$\frac{1}{\Delta t^2} \geq \frac{\alpha^2}{\Delta x^2}\sin^2\left(\frac{\bar{k}_x\Delta x}{2}\right) + \frac{\alpha^2}{\Delta z^2}\sin^2\left(\frac{\bar{k}_z\Delta z}{2}\right) \qquad \text{(C-16a)}$$

and

$$\frac{1}{\Delta t^2} \geq \frac{\beta^2}{\Delta x^2}\sin^2\left(\frac{\bar{k}_x\Delta x}{2}\right) + \frac{\beta^2}{\Delta z^2}\sin^2\left(\frac{\bar{k}_z\Delta z}{2}\right). \qquad \text{(C-16b)}$$

If equation C-16a is satisfied, equation C-16b is satisfied because $\alpha > \beta$ always. Consequently I need only equation C-16a. Because the largest value of either sine term in this equation is 1,

$$\Delta t \leq \frac{\Delta x}{\alpha\sqrt{2}}, \qquad \text{(C-17)}$$

for which I have set $\Delta x = \Delta z$, a common practice. This equation expresses the condition on Δt that must be satisfied for the solution to be numerically stable. In practice, I want Δt as large as possible to reduce the amount of computer computations, and the formula I use to calculate it is

$$\Delta t = \frac{\gamma\Delta x}{\alpha\sqrt{2}} \qquad \text{(C-18)}$$

where γ is some number slightly less than 1, say 0.95.

APPENDIX D
DISPERSION AND STABILITY, S_h-WAVES

In this appendix I derive, for S_h-waves, an equation to compute the dispersion of the phase velocity, an equation to compute the dispersion of the group velocity, and an equation that must be satisfied for stability of the solution. All derivations are new. Because the derivations are similar to those for P- and S_v-waves (Appendix C), I will omit the redundant details.

The components of the particle velocity and stress at location i, j and time k are expressed in terms of related components at location 0,0 and time 0:

$$\begin{pmatrix} v_y \\ \tau_{yz} \\ \tau_{xy} \end{pmatrix}_{i,j}^{k} = \begin{pmatrix} v_y \\ \tau_{yz} \\ \tau_{xy} \end{pmatrix}_{0,0}^{0} \exp\left[\imath\left(\bar{k}_x i\Delta x + \bar{k}_z j\Delta z - \omega k\Delta t\right)\right]. \tag{D-1}$$

Substitute this expression and similar expressions for the wave at $k+\frac{1}{2}$, $i+\frac{1}{2}$, etc. into equations 6a, 6b, and 6c. After some algebra the result is

$$0 = \mathbf{N}\begin{pmatrix} v_y \\ \tau_{yz} \\ \tau_{xy} \end{pmatrix}_{0,0}^{0} \exp\left[\imath\left(\bar{k}_x i\Delta x + \bar{k}_z j\Delta z - \omega k\Delta t\right)\right] \tag{D-2}$$

where the elements of **N** are

$$n_{11} = \frac{1}{\Delta t}\left(e^{\imath\omega\Delta t/2} - e^{-\imath\omega\Delta t/2}\right) \tag{D-3a}$$

$$n_{12} = \frac{1}{\rho\Delta x}\left(e^{\imath\bar{k}_x\Delta x/2} - e^{-\imath\bar{k}_x\Delta x/2}\right) \tag{D-3b}$$

$$n_{13} = \frac{1}{\rho\Delta z}\left(e^{\imath\bar{k}_z\Delta z/2} - e^{-\imath\bar{k}_z\Delta z/2}\right) \tag{D-3c}$$

$$n_{21} = \frac{\mu}{\Delta x}\left(e^{\imath\bar{k}_x\Delta x/2} - e^{-\imath\bar{k}_x\Delta x/2}\right)e^{-\imath\omega\Delta t/2}e^{-\imath\bar{k}_x\Delta x/2} \tag{D-3d}$$

$$n_{22} = \frac{1}{\Delta t}\left(e^{\imath\omega\Delta t/2} - e^{-\imath\omega\Delta t/2}\right)e^{-\imath\omega\Delta t/2}e^{\imath\bar{k}_x\Delta x/2} \tag{D-3e}$$

$$n_{23} = 0 \tag{D-3f}$$

$$n_{31} = \frac{\mu}{\Delta z}\left(e^{i\bar{k}_z \Delta z/2} - e^{-i\bar{k}_z \Delta z/2}\right)e^{-i\omega\Delta t/2}e^{i\bar{k}_z \Delta z/2} \tag{D-3g}$$

$$n_{32} = 0 \tag{D-3h}$$

$$n_{33} = \frac{1}{\Delta t}\left(e^{i\omega\Delta t/2} - e^{-i\omega\Delta t/2}\right)e^{-i\omega\Delta t/2}e^{i\bar{k}_z \Delta z/2} \tag{D-3i}$$

Computing the determinant of **N** and setting the result to zero yields the dispersion equation for a planar S_h-wave:

$$\frac{1}{\Delta t^2}\sin^2\left(\frac{\omega\Delta t}{2}\right) = \frac{\beta^2}{\Delta x^2}\sin^2\left(\frac{\bar{k}_x \Delta x}{2}\right) + \frac{\beta^2}{\Delta z^2}\sin^2\left(\frac{\bar{k}_z \Delta z}{2}\right). \tag{D-4}$$

This dispersion equation is easier to use if substitutions like those used for the S_V-wave are made; the result is

$$\frac{\beta_n}{\beta} = \frac{\sqrt{2}}{\pi\gamma H}\arcsin\left\{\frac{\gamma}{\sqrt{2}}\left[\sin^2(\pi H\cos\theta) + \sin^2(\pi H\sin\theta)\right]^{1/2}\right\}. \tag{D-5}$$

To calculate the dispersion of the group velocity, equation D-4 is differentiated with respect to k. After making the same substitutions that were make for the phase velocity, the group velocity of the calculated S_h-wave normalized by the true group velocity is

$$\frac{\beta_n^g}{\beta^g} = \frac{(\sin\theta + \cos\theta)\sin(2\pi H\cos\theta)}{2\cos(\frac{\beta_n}{\beta}\frac{\pi\gamma H}{\sqrt{2}})\left[\sin^2(\pi H\cos\theta) + \sin^2(\pi H\sin\theta)\right]^{1/2}} \tag{D-6}$$

The derivation for the condition for stability is identical to that for the P- and S_V-waves in all aspects except one: only one dispersion equation must be considered. Setting $\Delta x = \Delta z$, the final equation is

$$\Delta t \le \frac{\Delta x}{\beta\sqrt{2}}. \tag{D-7}$$

In practice I use

$$\Delta t = \frac{\gamma\Delta x}{\beta\sqrt{2}} \tag{D-8}$$

to calculate Δt where γ is some number slightly less than 1, say 0.95.

APPENDIX E
ANALYTICAL EQUATIONS FOR PARTICLE VELOCITIES, *P*- AND S_V-WAVE PROPAGATION

In this appendix, I derive exact, analytical equations for particle velocities on a free surface due to a linear, dilatational source. I use these particle velocities to determine the accuracy of the finite difference solutions for *P*-and S_V-wave propagation.

The derivation begins with the *x* and *z* components of the particle displacements on a free surface, $u_x(x,t)$ and $u_z(x,t)$, due to linear dilatational source for which the temporal part is a Heaviside step function. The dependent variables are the horizontal distance along the surface, *x*, and the time, *t*. Analytical expressions for these quantities are in equations 15 and 16 of Gilbert and Knopoff (1961) and will not be derived here. Since the ground is modeled as a linear system, the particle displacements due to a source for which temporal part is a delta function are the temporal derivative of $u_x(x,t)$ and $u_z(x,t)$ (Lathi, 1965, p. 406-408). The particle displacements due to an arbitrary excitation, $f(t)$, equal the convolution of the excitation with the impulse response:

$$u_x^f(x,t) = \int_{-\infty}^{\infty} f(t-\tau)\frac{du_x(x,\tau)}{d\tau}d\tau \qquad \text{(E-1)}$$

and

$$u_z^f(x,t) = \int_{-\infty}^{\infty} f(t-\tau)\frac{du_z(x,\tau)}{d\tau}d\tau \qquad \text{(E-2)}$$

(Lathi, 1965, p. 393-394). Both equations are integrated by parts, and the new terms outside the integrals go to zero because $f(t)$ is zero at $-\infty$ and ∞. To calculate the particle velocities, differentiate with respect to time and use the chain rule:

$$v_x^f(x,t) = \int_{-\infty}^{\infty} \left.\frac{d^2 f(p)}{dp^2}\right|_{p=t-\tau} u_x(x,\tau)d\tau \qquad \text{(E-3)}$$

and

$$v_z^f(x,t) = \int_{-\infty}^{\infty} \left.\frac{d^2 f(p)}{dp^2}\right|_{p=t-\tau} u_z(x,\tau)d\tau. \qquad \text{(E-4)}$$

APPENDIX F
ANALYTICAL EQUATIONS FOR PARTICLE VELOCITIES, S_h-WAVE PROPAGATION

In this appendix, I derive exact, analytical equations for particle velocities on a free surface due to a linear, body force source. I use these particle velocities to determine the accuracy of the finite difference solutions for S_h-wave propagation.

The derivation begins with the y component of the particle displacement, $u_y(x,z,t)$, caused by a linear source in an infinite homogeneous medium. The source is a body force acting impulsively in the y direction at the origin, and the displacement only depends upon the distance of the observation point from the origin. The analytical expression for $u_y(x,z,t)$ is given in Aki and Richards (1980, p. 226) and will not be repeated here. When a free surface exists, then the particle displacement may be considered the sum of the two components because the system is assumed to be linear. The first component, which I will designate $u_y^d(x,z,t)$, is the displacement due to the wave traveling directly between the source and the observation point, and it is computed using the formula for $u_y(x,z,t)$. The second component, which I will designate $u_y^r(x,z,t)$, is the displacement due to the wave reflected from the free surface. Because an S_h-wave that is reflected from a free surface has the same amplitude as the incident wave, $u_y^r(x,z,t)$ can be computed using the formula for $u_y(x,z,t)$ if the total distance traveled by the reflected wave is used. The particle displacement due to an arbitrary excitation, $f(t)$, equals the convolution of the excitation with the impulse response:

$$u_y^f(x,z,t) = \int_{-\infty}^{\infty} f(t-\tau)\left[u_y^d(x,z,\tau) + u_y^r(x,z,\tau)\right]d\tau. \qquad \text{(F-1)}$$

To calculate the particle velocities, differentiate with respect to time and use the chain rule:

$$v_y^f(x,z,t) = \int_{-\infty}^{\infty} \left.\frac{f(p)}{dp}\right|_{p=t-\tau} \left[u_y^d(x,z,\tau) + u_y^r(x,z,\tau)\right]d\tau\ . \qquad \text{(F-2)}$$

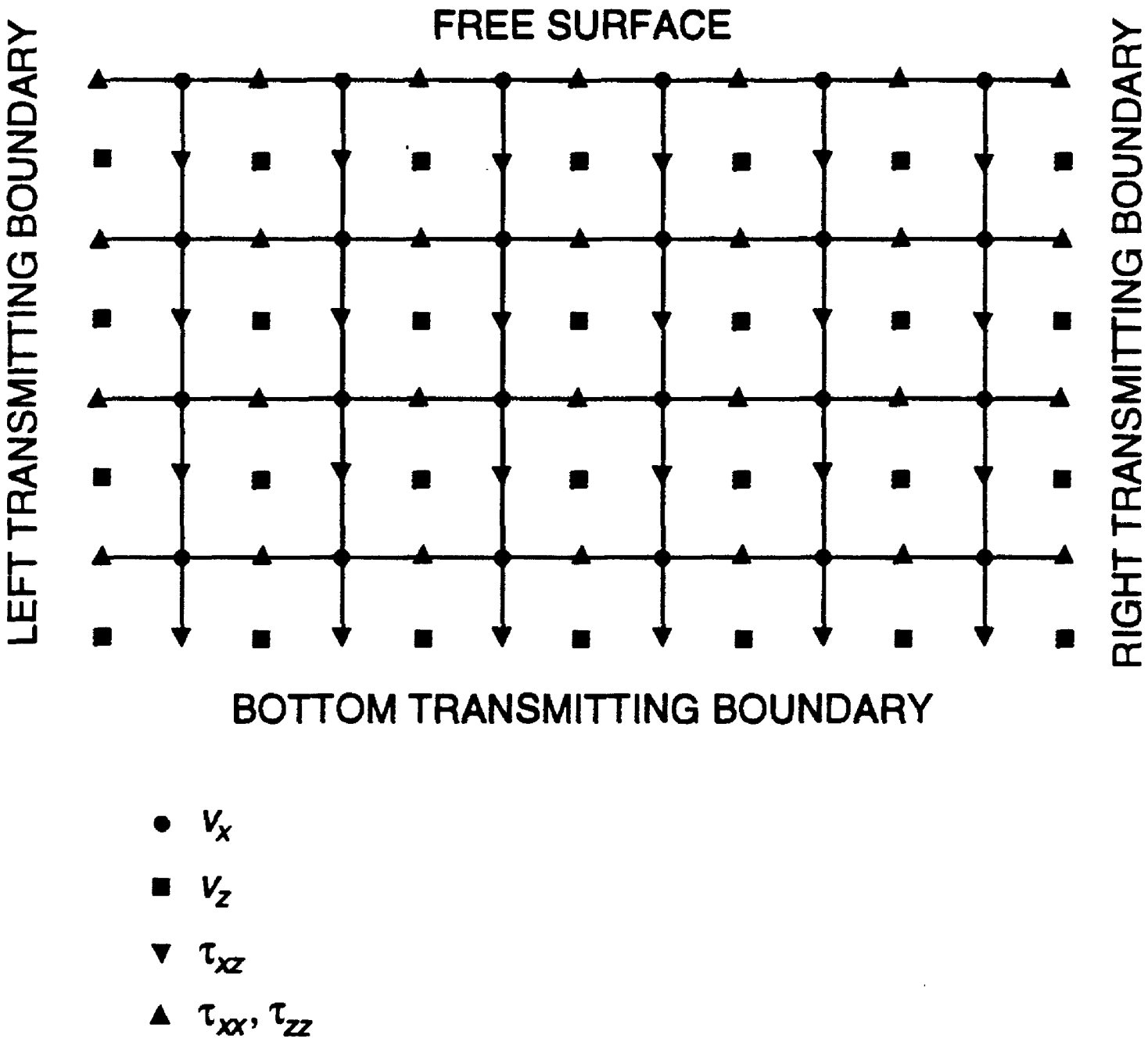

Figure 1. Grid used to simulate *P*- and S_V-wave propagation.

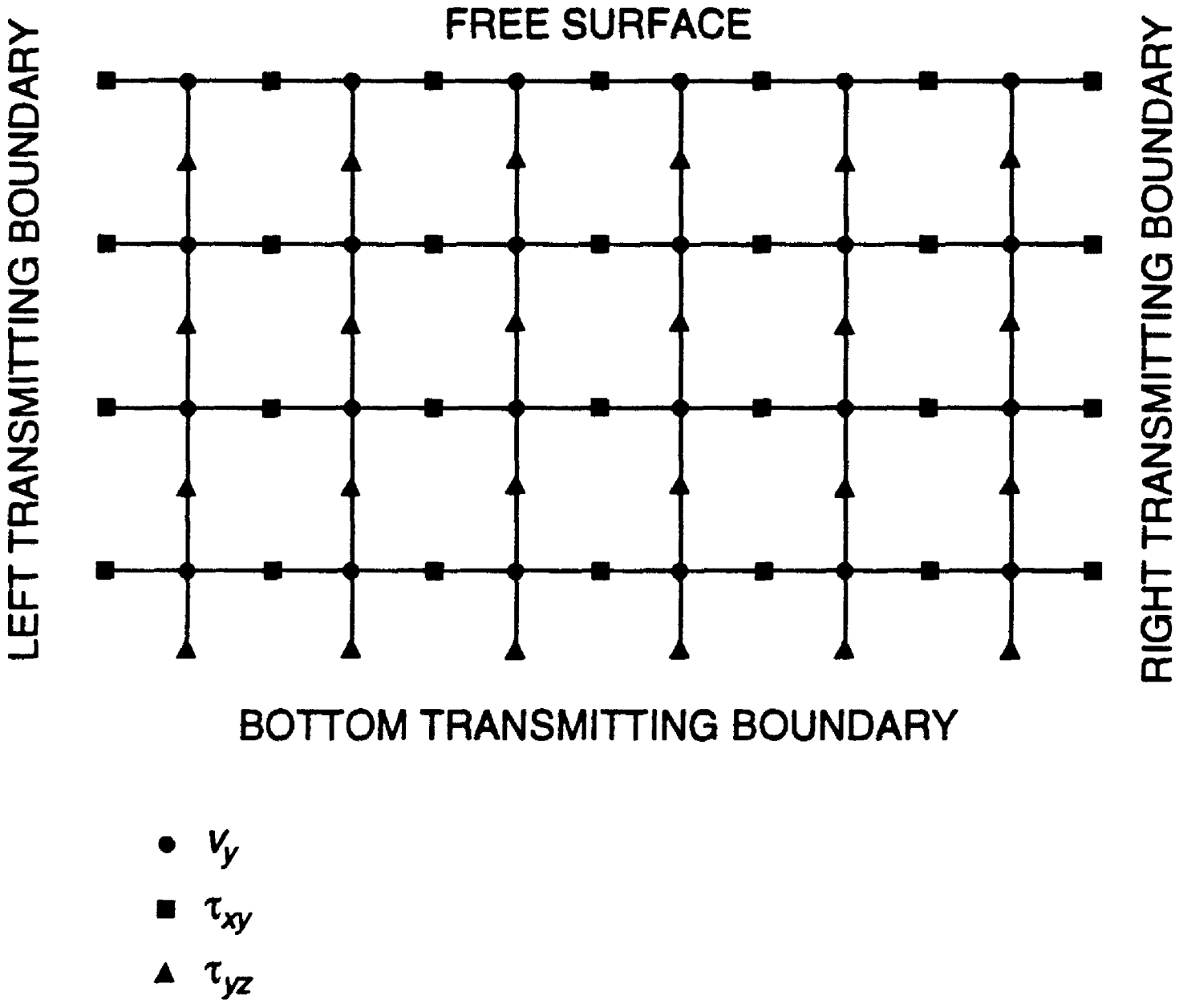

Figure 2. Grid used to simulate S_h-wave propagation.

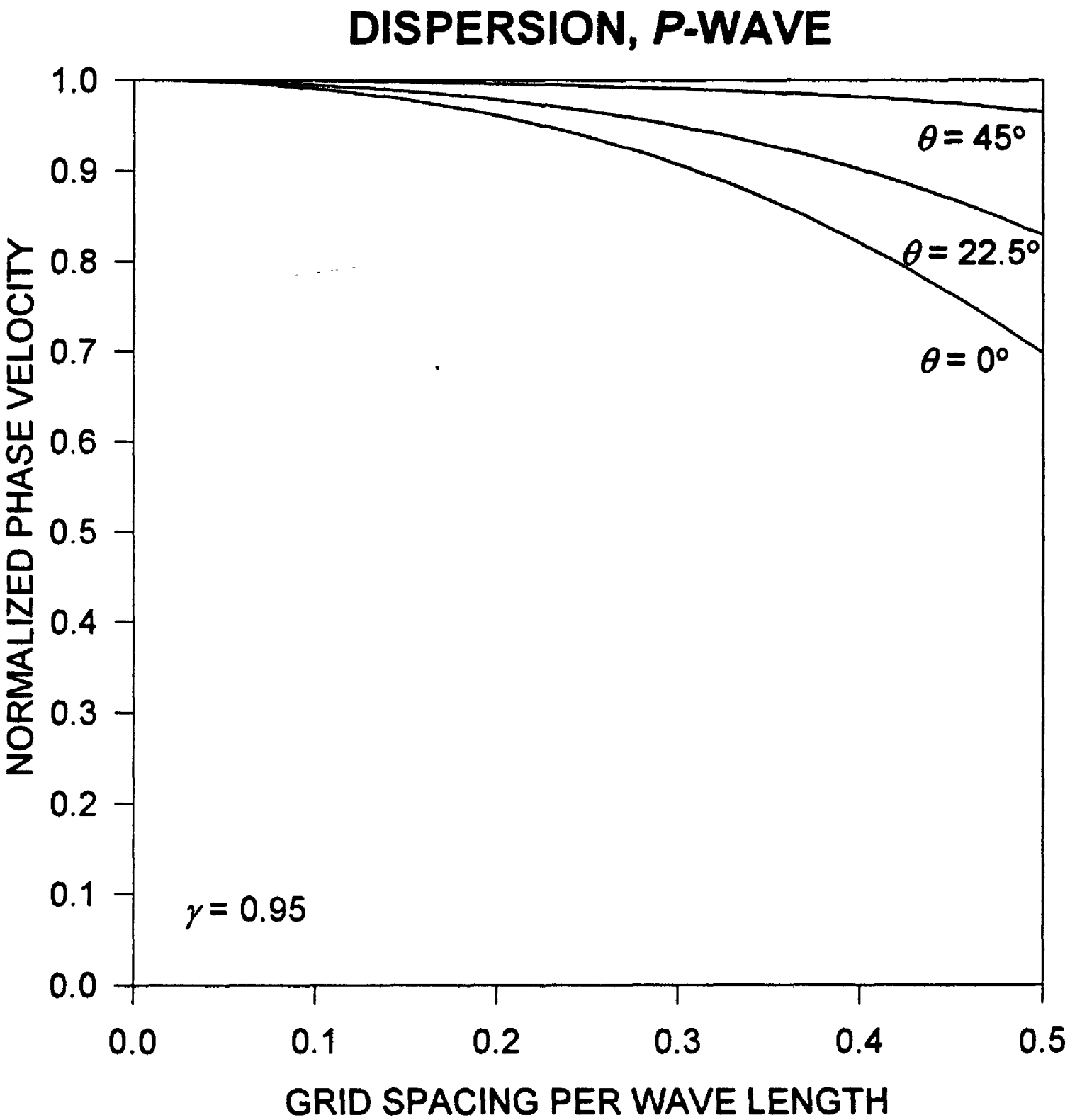

Figure 3. Normalized phase velocity of a *P*-wave simulated on a staggered finite difference grid with different spacings. The angle of propagation, θ, is measured from the the horizontal.

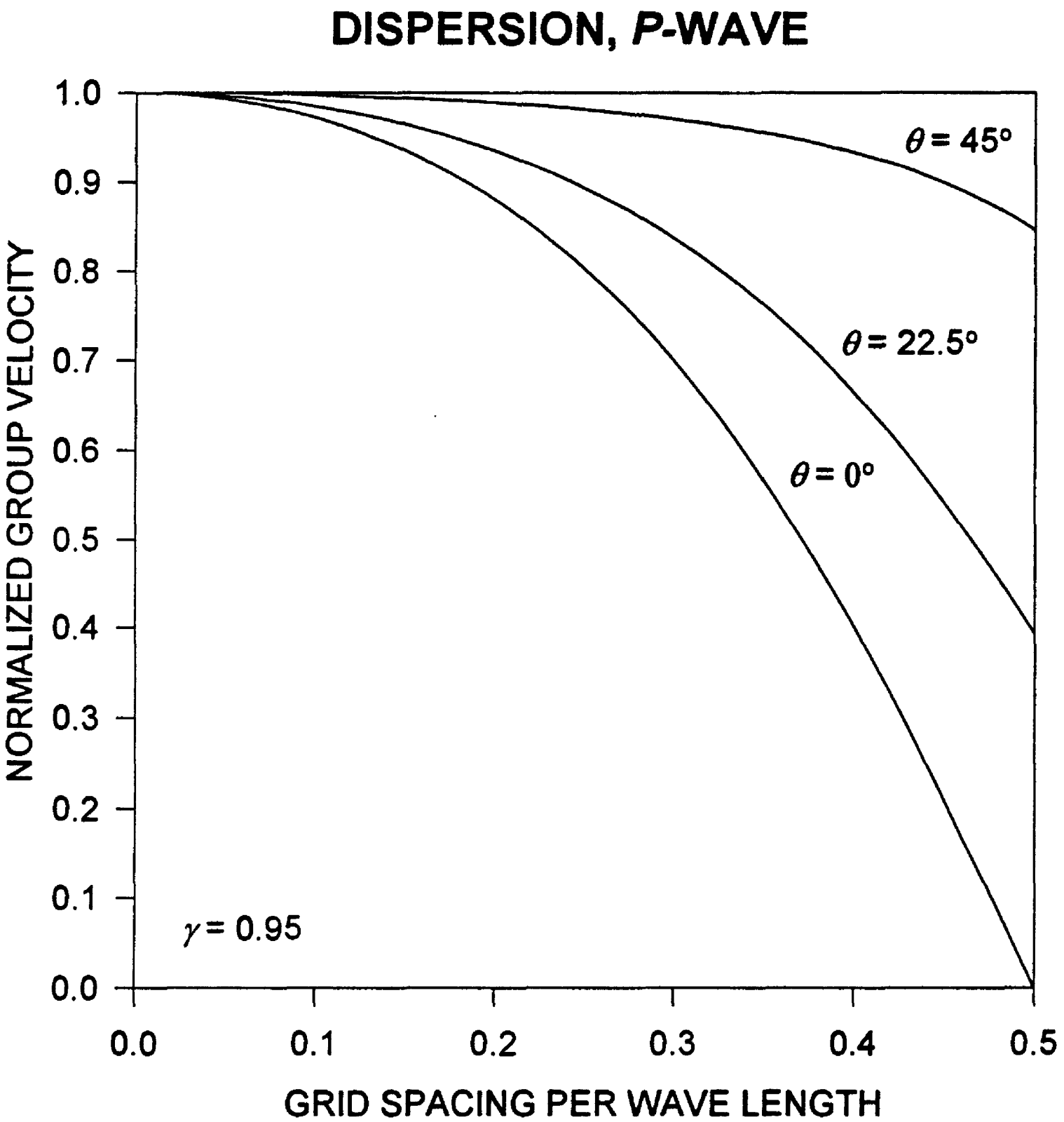

Figure 4. Normalized group velocity of a *P*-wave simulated on a staggered finite difference grid with different spacings. The angle of propagation, θ, is measured from the the horizontal.

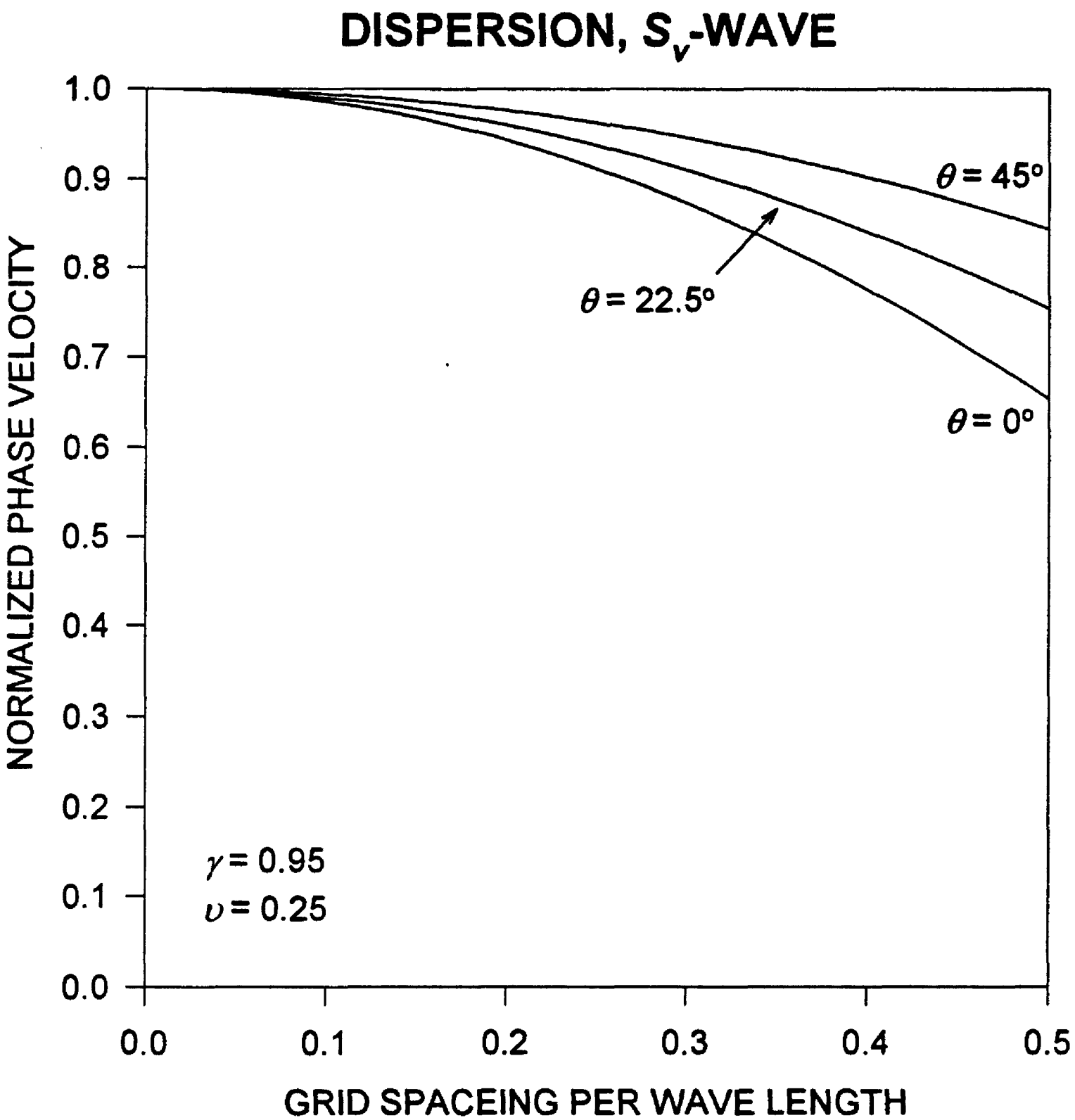

Figure 5. Normalized phase velocity of a S_v-wave simulated on a staggered finite difference grid with different spacings. The angle of propagation, θ, is measured from the the horizontal. Poisson's ratio is 0.25.

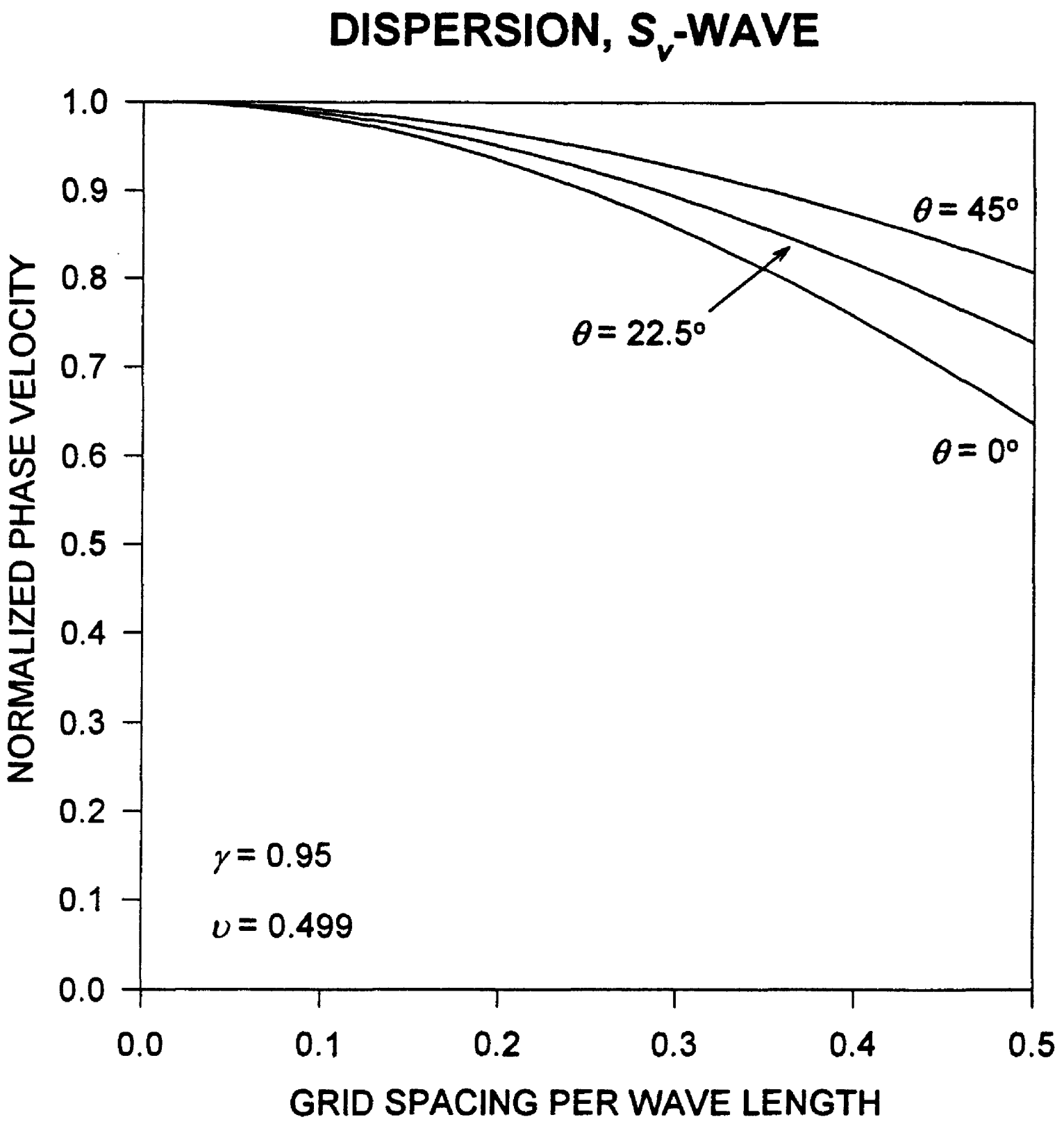

Figure 6. Normalized phase velocity of a S_V-wave simulated on a staggered finite difference grid with different spacings. The angle of propagation, θ, is measured from the the horizontal. Poisson's ratio is 0.499.

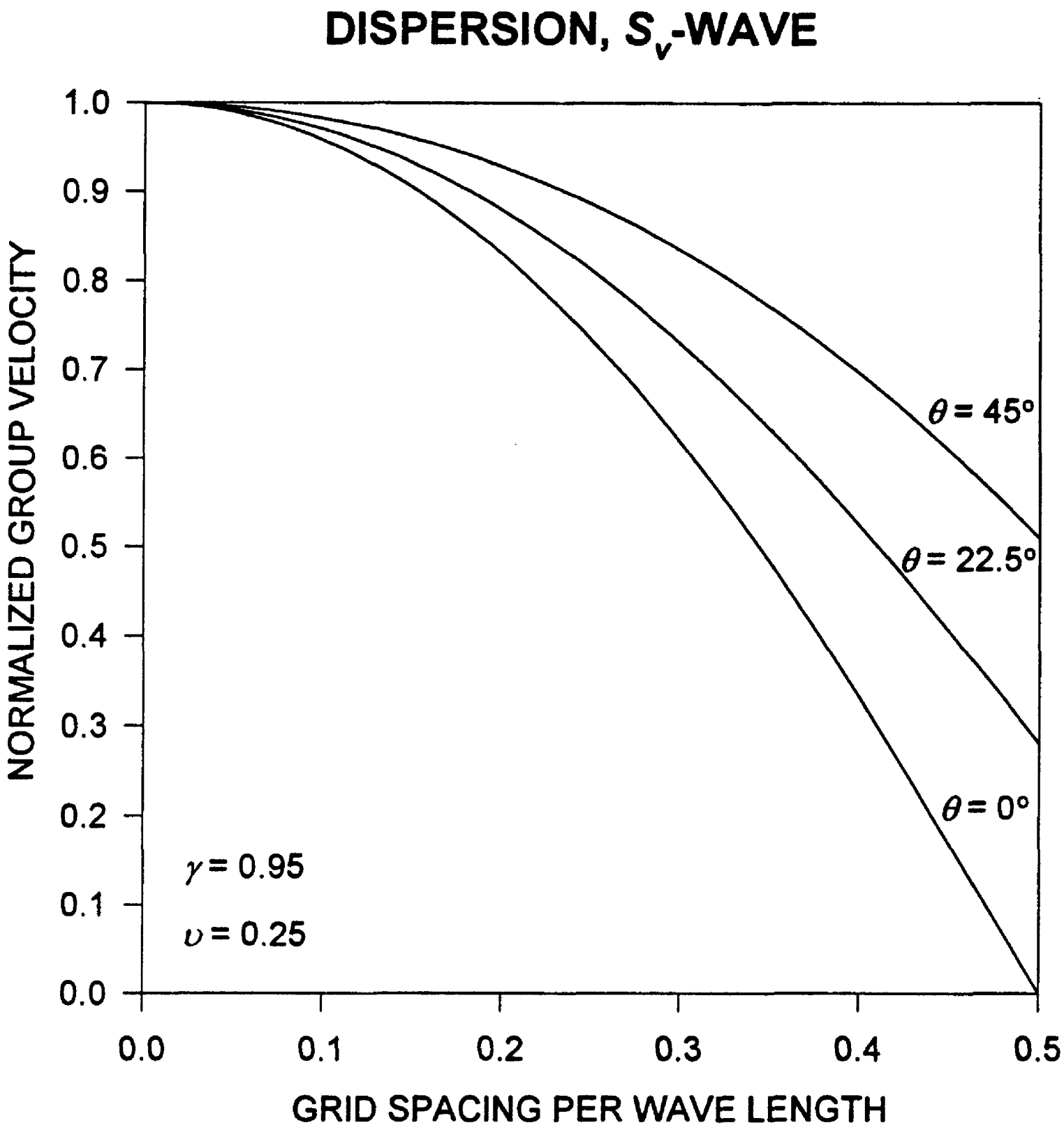

Figure 7. Normalized group velocity of a S_V-wave simulated on a staggered finite difference grid with different spacings. The angle of propagation, θ, is measured from the the horizontal. Poisson's ratio is 0.25.

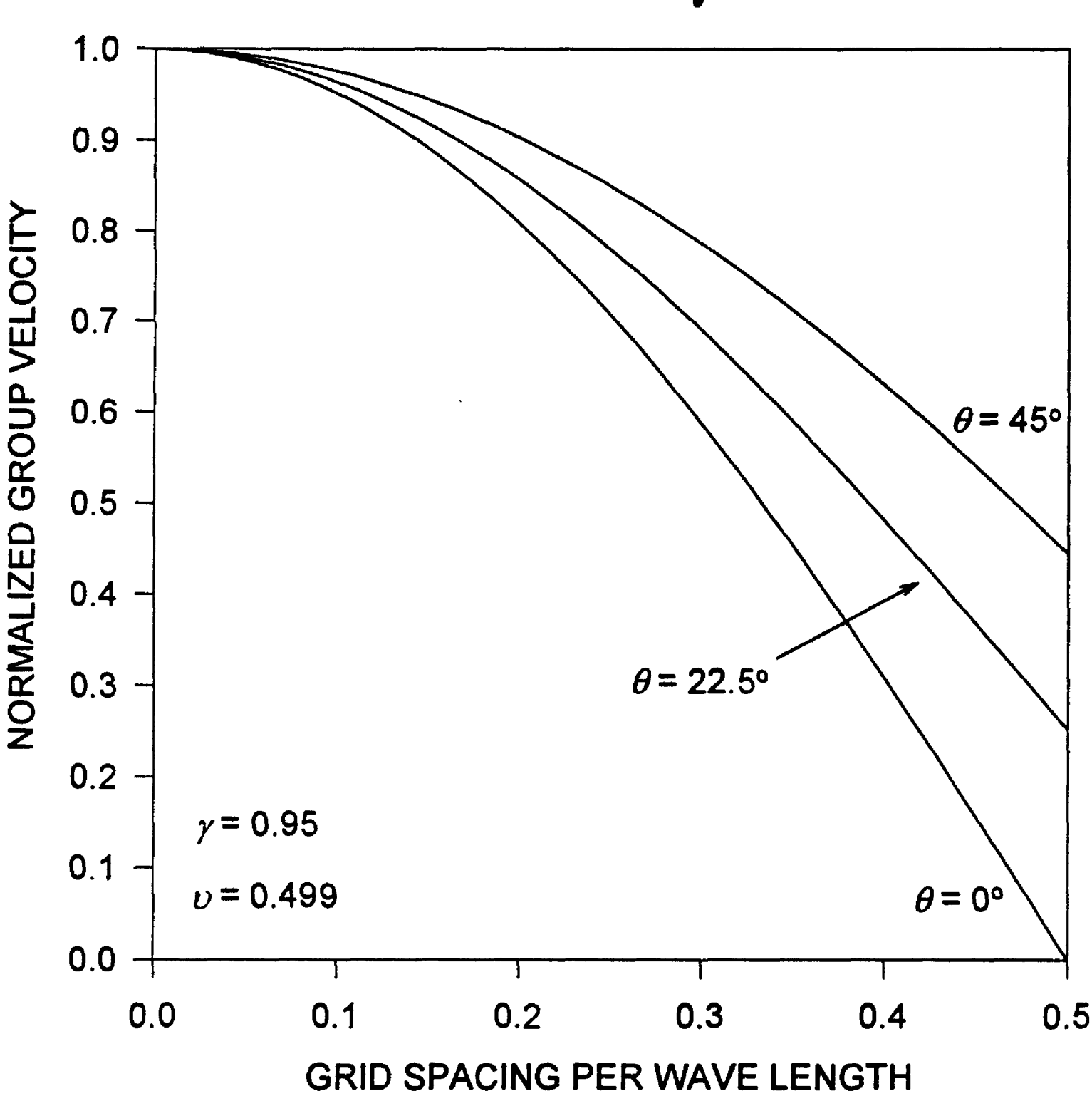

Figure 8. Normalized group velocity of a S_V-wave simulated on a staggered finite difference grid with different spacings. The angle of propagation, θ, is measured from the the horizontal. Poisson's ratio is 0.499.

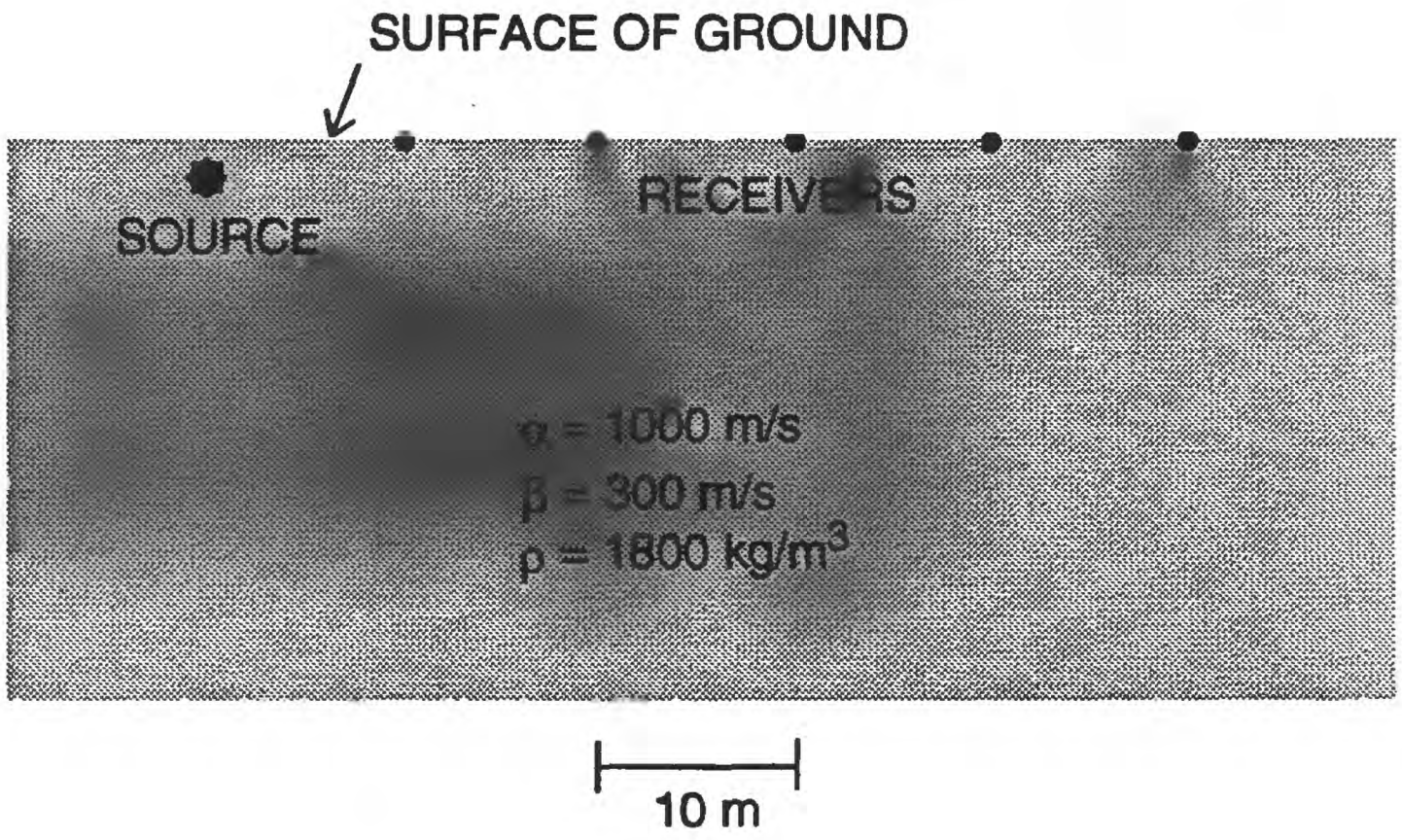

Figure 9. Model and source-receiver geometry used to test the accuracy of the finite difference simulation of P- and S_V- wave propagation.

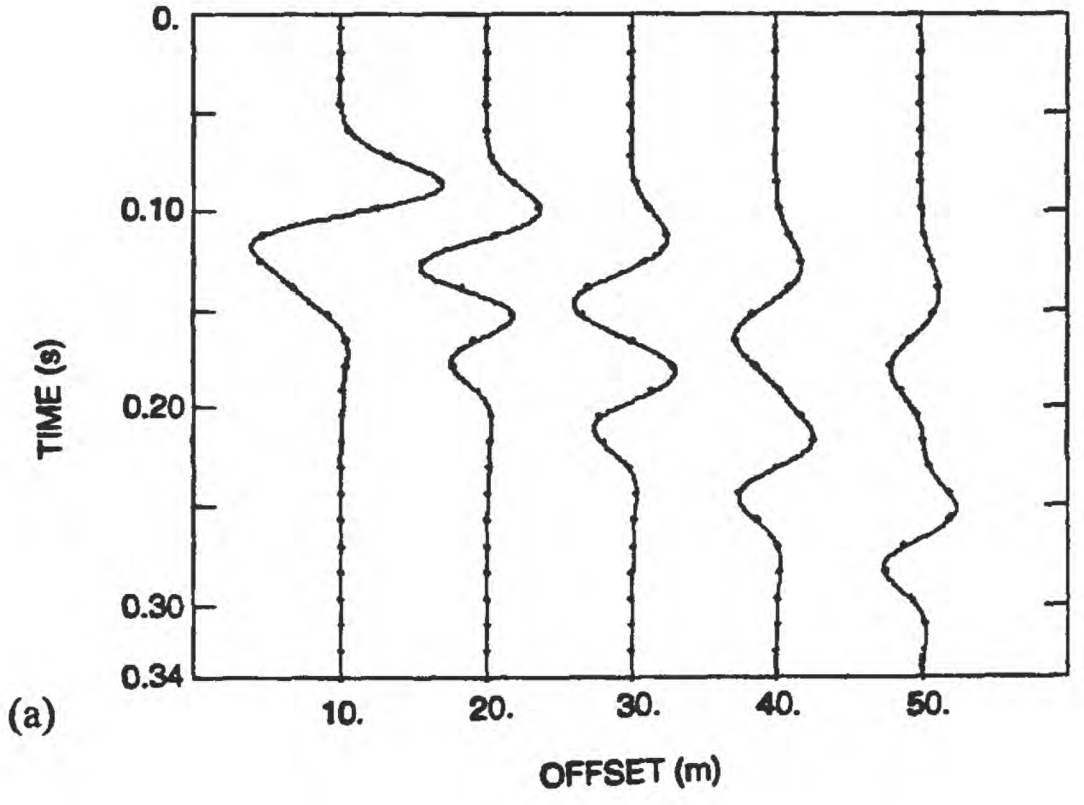

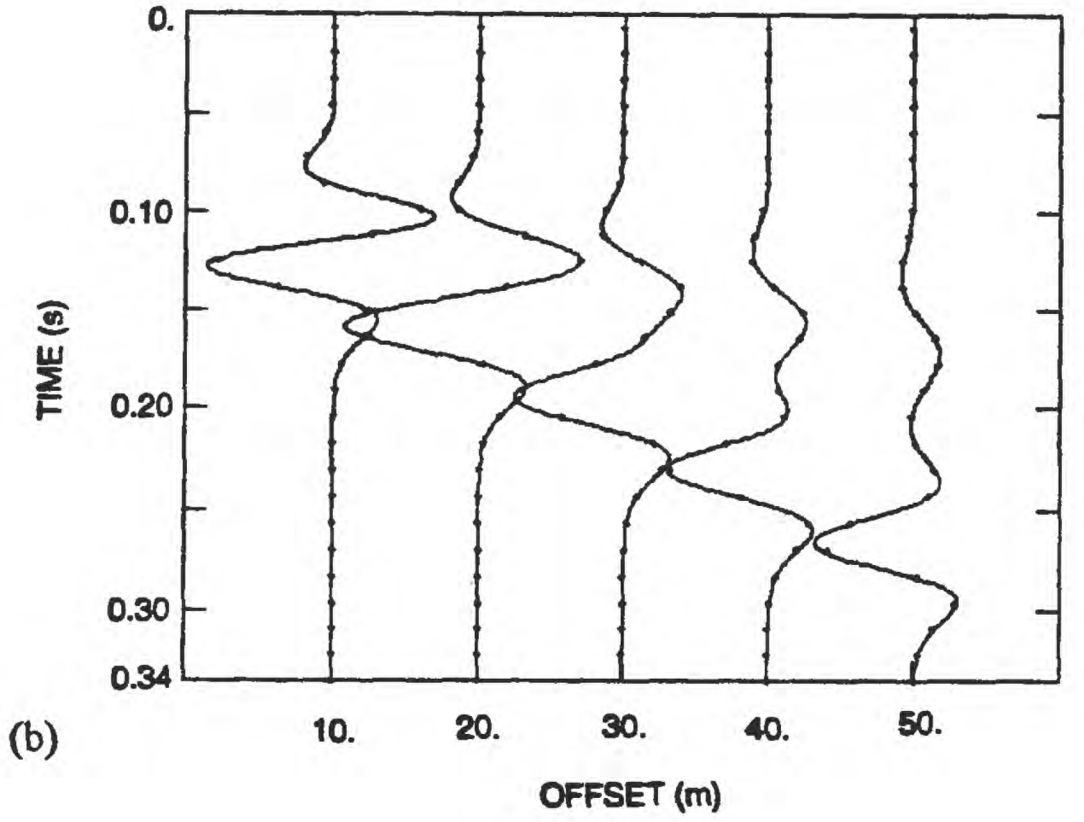

Figure 10. (a) x and (b) z components of the particle velocity for the model in Figure 9. The finite difference solution is represented by the solid lines; the exact, analytical solution by the dots.

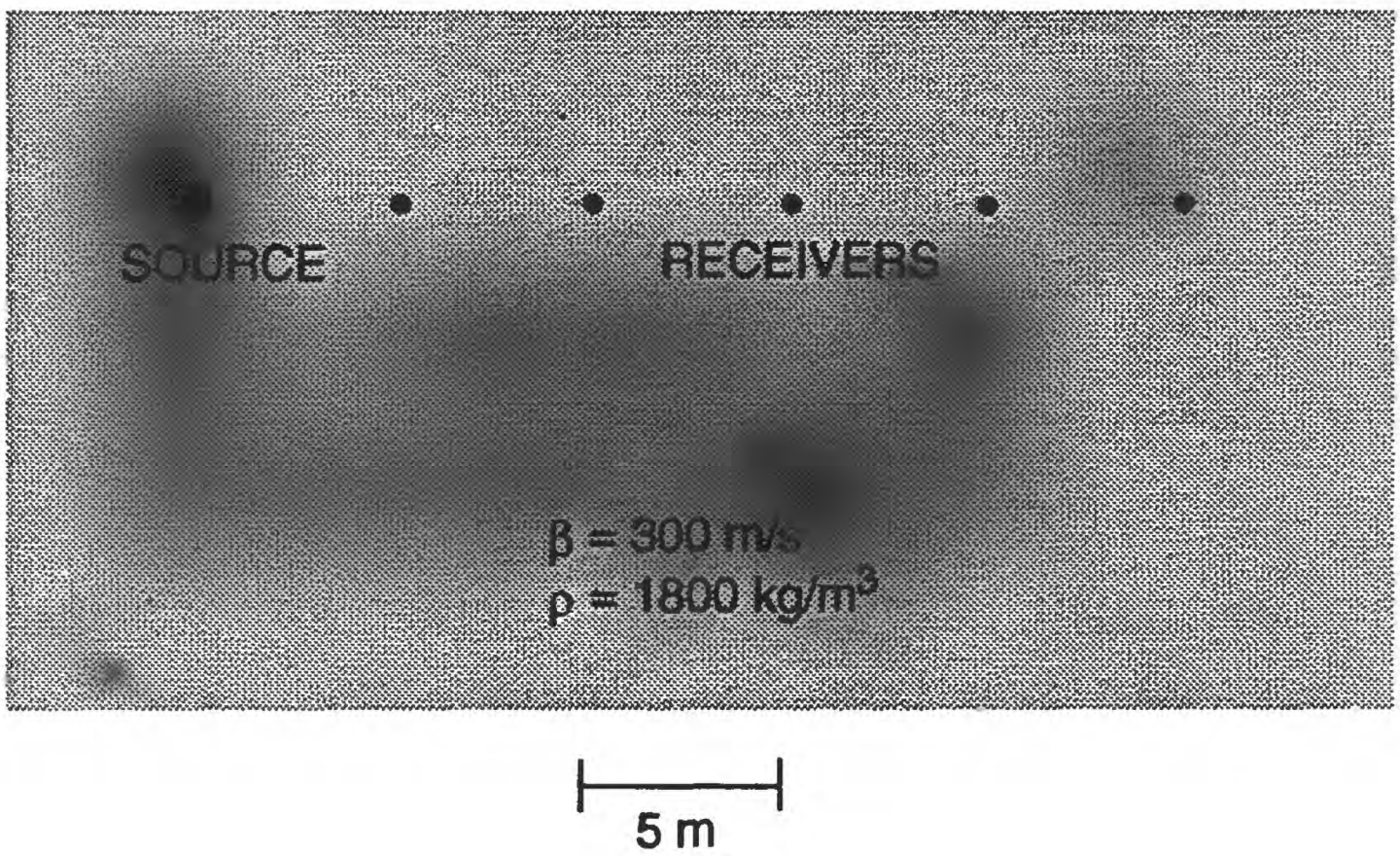

Figure 11. Model and source-receiver geometry used to test the accuracy of the finite difference simulation of S_h- wave propagation.

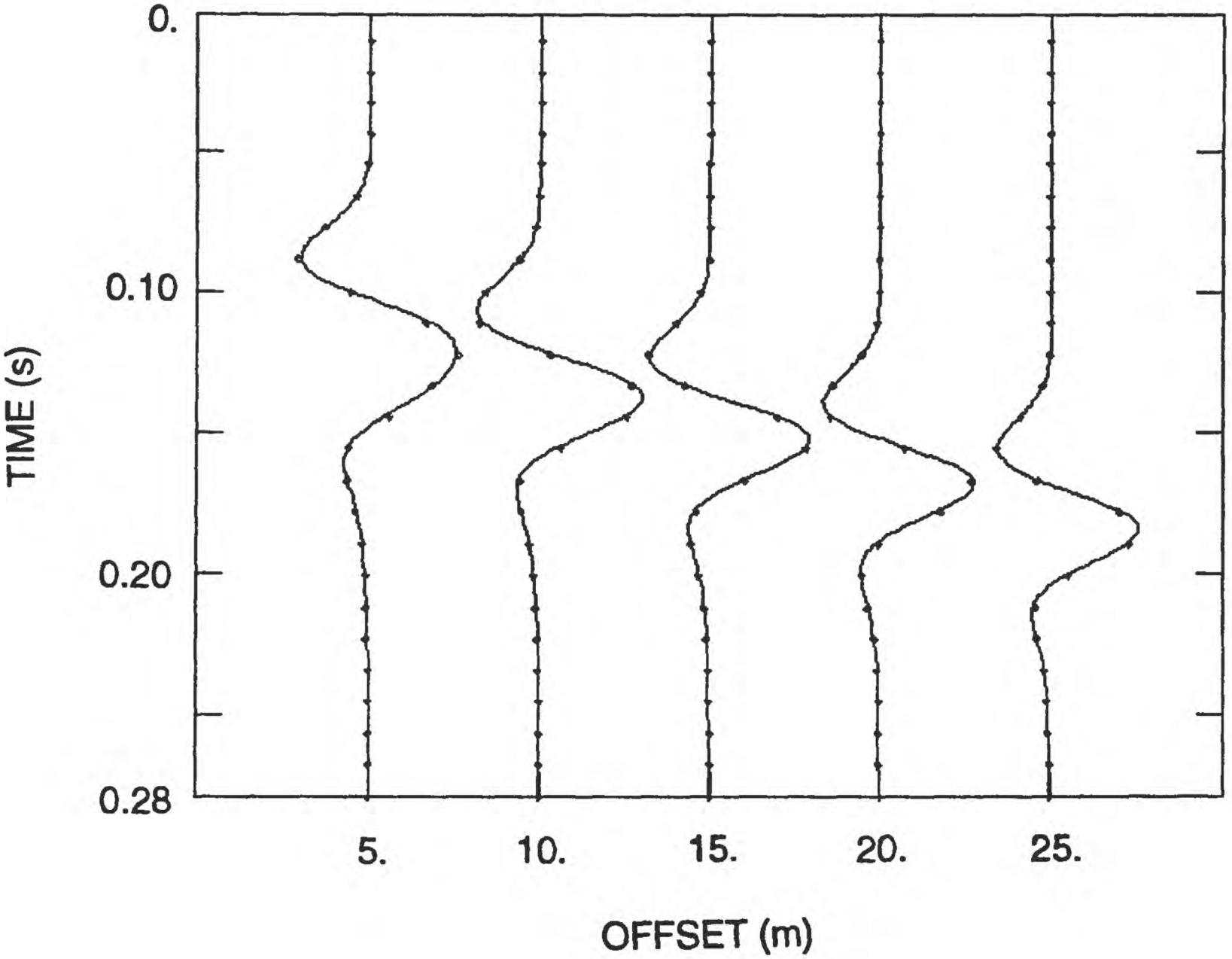

Figure 12. *y* component of the particle velocity for the model in Figure 11. The finite difference solution is represented by the solid lines; the exact, analytical solution by the dots.